Hindawi
Journal of Advanced Transportation
Volume 2019, Article ID 9723042, 13 pages
https://doi.org/10.1155/2019/9723042

Research Article

Distributed H_∞ Control of AVs Interacting by Uncertain and Switching Topology in a Platoon

Feng Gao,[1] **Dongfang Dang**,[1] **Qiuxia Hu**,[1] **and Yingdong He**[2]

[1]*School of Automotive Engineering, Chongqing University, Chongqing, China*
[2]*Mechanical Engineering, University of Michigan, MI 48109, USA*

Correspondence should be addressed to Feng Gao; gaofeng1@cqu.edu.cn

Received 17 August 2018; Revised 22 January 2019; Accepted 28 January 2019; Published 3 March 2019

Academic Editor: Yair Wiseman

To overcome the challenges arising from the weakness of wireless communication, this paper presents a distributed $\boldsymbol{H}_\infty$ control method for multi-AVs connected by an uncertain and switching topology in a platoon. After compensating for the powertrain nonlinearities, we model the node dynamics as a linear uncertain system. By applying the eigenvalue decomposition and linear transformation, the platoon system is decomposed to multiple low order subsystems depending on the eigenvalues of the topological matrix. The sufficient condition ensuring the robust performance of the platoon is presented by using the invariant of signal amplitude of the linear transformation. Then a numerical method is provided to solve the state feedback controller by using the LMI scheme. Only the bounds of the topological eigenvalues are necessary for this new synthesis method and the designed controller can govern the platoon composed of disturbed nodes and interacting by uncertain even switching topologies in a satisfactory way. The effectiveness of this distributed $\boldsymbol{H}_\infty$ control strategy is validated by comparative bench tests between nominal and disturbed conditions.

1. Introduction

Many traffic performances, e.g., driving safety, fuel consumption, traffic congestion, and air pollution, can be improved by platooning, which has attracted extensive interests since the PATH program in 1980s [1–3]. Recently some demos have been carried out in the real world, e.g., the SARTRE in Europe [4]. In the past years, many issues about platooning have been studied, such as how to consider the nonlinearities and dynamics of powertrain [5], the influences of spacing policy [6, 7], homogeneity and heterogeneity [8], and asymptotical and string stability [9]. Many advanced control methods have been applied to platoon control to achieve better performances [2, 10–12].

These earlier studies mainly consider the radar-based or centralized control systems, whose interaction topologies are simple and quite limited. Recently because of the rapid development of wireless communication, it is a trend to apply vehicle-to-vehicle communication (V2V), such as dedicated short range communication (DSRC), to automated vehicles (AVs) [13]. The application of V2V generates a variety of new interaction topologies such as multiple-predecessor following type. Comparing with the earlier systems, new challenges arise due to the topological variety including the robustness of information connections, the dimension, and structure of interaction topologies. It becomes even critical, when there exist time delay and packet loss in wireless communication.

From the perspective of multiagent control system, a platoon connected by V2V can be considered as a dynamical network with one dimension, in which each node only uses its neighboring information. When the nodes are interacting by a symmetrical information flow called "undirected topology", the network can be decoupled to multisystems with lower order, whose open loop gain depends on the topological eigenvalues. With this approach, Zheng et al. gave out the asymptotic stability condition of homogeneous platoons and introduced a method to improve the stability margin via topological selection and control adjustment [14]. To overcome the drawback of homogeneous state feedback controller, a heterogeneous feedback controller is further designed to ensure string stability of platoons interacted by bidirectional topology in [15, 16]. With the leader-follower

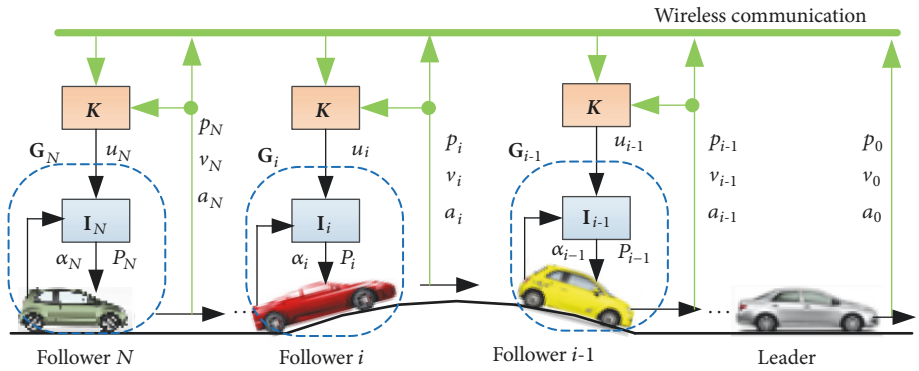

FIGURE 1: The heterogeneous platoon influenced by environments and interacting by uncertain topology.

topology, the collision avoidance ability is further considered in [17].

In practice, node dynamics may be affected by many factors such as vehicle type, environmental resistance, and working condition. To deal with such uncertainties, Wang et al. proposed a linear matrix inequality (LMI) method to optimize the state feedback controller for multi-AVs interacted by preknown and fixed topologies [18]. Gao et al. further presented a robust control method for heterogeneous platoons interacted by undirected topologies [19]. This synthesis method has been extended to general, but eigenvalue decomposition known topologies in [20]. The problem of actuar saturation and velocity absent is considered by using the consensus theory [21]. To relax the contradiction between performances and uncertainties of the system with a fixed parameter controller, adaptive algorithms have also been applied to platoon interacting by bidirectional [22] or leader-follower topologies [23], respectively.

The aforementioned studies all assume that the wireless connection is stable and will not be stopped. In practice, a fixed interaction topology is rather rare because of the following [24]. (a) The quality of communication is significantly degraded by adverse environments, leading to packet loss, broken link, channel delay, etc. (b) The topological structure and dimension is spatial-temporally varying due to cut-in/off of vehicles from adjacent lanes. There are some achievements about the influence of time delay, packet loss, and quantization error in wireless communication on platoon performances. By simplifying the node dynamics to a second-order integral equation, Wang et al. studied the influence of the random changing network structure on platoon dynamics by using a weighted and constrained seeking framework [25]. Gao et al. designed a local string stable $\boldsymbol{H}_\infty$ controller for a heterogeneous platoon, simultaneously considering vehicle uncertainties and identical communication delays [26]. Moreover an adaptive distributed sliding mode control strategy was proposed in [27] to simutaneously deal with the nonlinearieties and uncertainties of node dynamics for platoon interacted by uncertain but time-invariat topologies. Wen et al. considered a more complicated condition that the topology switches and the control input misses ocassionally [28]. With the central control structure, the model predictive control theory was used to design a robust longitudinal controller of platoon with model uncertaitnies and time delay in [29]. From the view point of consensus control, Bernardo et al. further proposed a distributed strategy to deal with the time varying and heterogeneous communication delays by using the Lyapunov-Razumikhin functions [30, 31].

To synthetically deal with the uncertainties in vehicle dynamics and interaction topologies, this paper presents a synthesis method for distributed $\boldsymbol{H}_\infty$ control of platoon. By compensating the nonlinearities of vehicle dynamics with an inverse model, we model the node dynamics as a third-order system with parametric uncertainties. Based on the close loop dynamics of platoon controlled by a identical state feedback controller, the platoon is firstly decoupled to multisubsystems with lower order by making eigenvalue decomposition on the interaction topology and the linear transformation. Based on this decoupled system, the sufficient condition, which ensures the required robust performance of platoon and depends on topological eigenvalues, is presented by using the invariance property of signal amplitude of the linear transformation. Then a numerical method based on the LMI theory is provided to solve the state feedback controller. Its advantage is that the entry values of topological matrix are not necessary and only their bounds need to be known even for random switching topologies. The effectiveness of this distributed $\boldsymbol{H}_\infty$ control strategy is validated by comparative bench tests under both nominal and disturbed conditions.

2. Problem Description

The studied platoon includes N+1 vehicles, i.e., a leader (indexed by 0) and N followers (indexed by $i = 1, \cdots, N$ accordingly), shown in Figure 1. Each follower uses a hierarchical control structure including an upper layer controller $\boldsymbol{K}$ and a lower layer inverse model $\mathbf{I}_i$. The former is designed for formation control, while the latter is to compensate for the nonlinearities of powertrain dynamics.

The objective of platoon control is to track the leader speed while maintaining a specified clearance governed by

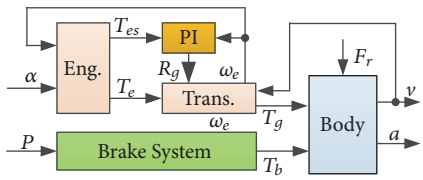

Figure 2: Vehicle longitudinal dynamics including a combustion engine, a continuous variable transmission (CVT), a hydraulic braking system, and a mechanical body.

the constant spacing policy for a high traffic capacity [7, 15, 16]:

$$\begin{aligned} p_i(t) - p_0(t) &= i \cdot d_0 \\ v_i(t) &= v_0(t), \quad i = 1, \cdots N \end{aligned} \tag{1}$$

where $p_i(t)$, $v_i(t)$ are the position and velocity of follower i and d_0 is the desired gap, and $v_0(t)$ is the speed of leader. Other spacing policies, such as the constant time-headway which is better accord with driver behaviors, are not considered here [6].

2.1. Vehicle Longitudinal Dynamics. The vehicles are assumed to have the same powertrain and braking configuration depicted by Figure 2 [32].

The engine is modeled by its steady torque characteristic with a first-order system for its dynamics:

$$\begin{aligned} \dot{T}_{eoi}(t) &= \frac{\left[T_{esi}(t) - T_{eoi}(t)\right]}{t_e} \\ T_{esi}(t) &= MAP\left[\alpha_i(t), \omega_{ei}(t)\right] \\ \dot{\omega}_{ei}(t) &= \frac{\left[T_{eoi}(t) - T_{ei}(t)\right]}{J_e} \end{aligned} \tag{2}$$

where $\alpha_i(t)$ is the throttle angel, $\omega_{ei}(t)$ is the engine speed, $T_{esi}(t)$ and $T_{eoi}(t)$ are the steady and dynamic engine torque, $T_{ei}(t)$ is the output torque, $MAP(\cdot)$ is the steady torque characteristic, t_e is the time constant, and J_e is the rotating inertia of flywheel.

The CVT is controlled by a proportional-integral (PI) controller with the engine speed tracking error as feedback:

$$\begin{aligned} T_{gi}(t) &= \eta_t R_0 R_{gi}(t) T_{ei}(t) \\ \omega_{ei}(t) &= \frac{R_0 R_{gi}(t) v_i(t)}{r} \\ R_{gi}(t) &= K_P e_{\omega i}(t) + K_I \int e_{\omega i}(t)\, \mathrm{d}t \\ e_{\omega i}(t) &= TS\left[T_{esi}(t)\right] - \omega_{ei}(t) \end{aligned} \tag{3}$$

where $T_{gi}(t)$ is the output torque of CVT, $R_{gi}(t)$ is the speed ratio, $TS(\cdot)$ describes the relationship between $T_{esi}(t)$ and corresponding engine speed achieving optimal fuel rate, η_t is the mechanical efficiency, R_0 is the speed ratio of final drive, r is the tyre radius, and K_P and K_I are the proportional and integral gain of PI controller.

The braking system is modeled by a first-order system:

$$\dot{T}_{bi}(t) = \frac{\left[K_b P_i(t) - T_{bi}(t)\right]}{t_b} \tag{4}$$

where $T_{bi}(t)$ is the braking torque, $P_i(t)$ is the braking pressure, and K_b and t_b are the gain and time constant.

The vehicle is assumed to run on dry and alphabet roads; therefore some reasonable Assumptions are made to build a concise but nonlinear model including the following [16, 26]. (a) The vehicle body is considered to be rigid and left-right symmetric. (b) The pitch and yaw motions are neglected. (c) The tire slip is negligible and the wheel motion are lumped into the powertrain dynamics. Then the body dynamics is modeled as

$$\begin{aligned} \dot{p}_i(t) &= v_i(t), \\ \dot{v}_i(t) &= a_i(t) \\ a_i(t) &= \frac{\left\{r\left[T_{gi}(t) - T_{bi}(t)\right] - F_{ri}(t)\right\}}{M_i} \\ F_{ri}(t) &= F_{fi}(t) + F_{wi}(t) \\ F_{wi}(t) &= C_a\left[v_i(t) + v_w(t)\right]\left|v_i(t) + v_w(t)\right| \\ F_{fi}(t) &= M_i g\left(f_i \cos\rho + \sin\rho\right) \end{aligned} \tag{5}$$

where $a_i(t)$ is the acceleration, $v_w(t)$ is the wind speed, ρ is the road slope, M_i is the lumped vehicle mass, C_a is the wind resistance coefficient, g is the gravity acceleration, and f_i is the rolling resistance coefficient.

2.2. Inverse Vehicle Model. One challenge for control is the salient nonlinearities of powertrain dynamics, which can be linearized by feedback [15] or compensated for by an inverse models [5]. Here the following inverse model $\mathbf{I}_i$ is used to compensate for the nonlinearities:

$$\begin{aligned} &\alpha_i(t) \\ &= \begin{cases} 0, & \text{if } u_i(t) \le a_{th}\left[v_i(t)\right] \\ MAP^{-1}\left[\dfrac{T_{di}(t)}{\left(\eta_t R_0 R_{gi}(t)\right)}, \omega_{ei}(t)\right], & \text{else} \end{cases} \\ &P_i(t) = \begin{cases} \dfrac{T_{di}(t)}{K_b}, & \text{if } u_i(t) < a_{th}\left[v_i(t)\right] \\ 0, & \text{else} \end{cases} \\ &T_{di}(t) = r\left[M_0 u_i(t) + C_a v_i^2(t) + M_0 g f_0\right] \end{aligned} \tag{6}$$

where M_0 and f_0 are the nominal values of lumped vehicle mass and rolling resistance coefficient and $a_{th}(\cdot)$ is the coasting acceleration. The parameter values of vehicle dynamical model and its inverse are shown in Table 1.

2.3. Uncertain Linear Model of Node Dynamics. To synthesize the upper layer controller for formation control of platoon, a

Table 1: Parameter values of vehicle model.

Symb.	Description	Units	Range	Norm
t_e	engine time constant	s	0.2~0.4	-
J_e	flywheel inertia	kg·m^2	-	0.212
η_t	mechanical efficient	-	-	0.7
R_0	final drive ration	-	-	2.86
R_{gi}	ratio of CVT	-	0.326~2.25	-
K_P	proportional factor	-	-	0.02
K_I	integral factor	-	-	0.001
K_b	braking system factor	N·m/MPa	-	800
t_b	braking time constant	s	-	0.1
r	tyre radius	m	-	0.3
M	lumped vehicle mass	kg	1200~2100	1645
C_a	wind resistance coefficient	kg/m	-	0.43
f	roll resistance coefficient	-	0.015~0.025	0.02
ρ	road slope	%	-10~10	0
v_w	wind speed	m/s	-5~5	0
τ	drivetrain time constant	s	0.14~0.33	/
k	drivetrain gain	-	0.86~0.99	0.935
ε	equivalent disturbance	-	-0.22~0.08	/

model for control is needed to describe the dynamics of lower level system composed of the vehicle longitudinal dynamics and its inverse model. Since the nonlinearities of powertrain dynamics are compensated for by its inverse model, the following equations with two parameters and one disturbance to strike a balance between conciseness and accuracy is used to describe node dynamics [5, 15]:

$$\begin{aligned} \dot{p}_i(t) &= v_i(t), \\ \dot{v}_i(t) &= a_i(t) \\ \dot{a}_i(t) &= -\frac{a_i(t)}{\tau_i} + k_i u_i(t) + \varepsilon_i \end{aligned} \tag{7}$$

where τ_i is the time constant, k_i is the gain, and ε_i is the equivalent external disturbance. These parameters in (7) are influenced by running conditions and environmental resistances. Matlab toolbox *ident* is used to estimate their values at different running conditions and vehicle parameter values (see [5] for details).

The considered uncertain parameters are vehicle mass, time constant of engine, rolling resistance coefficient, wind speed, and road slope. During identification, a uniform random signal is used to excite the node dynamics; each uncertain variable is set to its maximum, minimum, and medium value, respectively, which is shown together with the idetified parameter limits in Table 1.

From (7) and its parameter uncertaintes shown in Table 1, to normalize the parametric uncertainties, the uncertain linear model of $\mathbf{G}_i$ is constructed as [33, 34]

$$\begin{aligned} \dot{\boldsymbol{x}}_i(t) = \boldsymbol{A}\boldsymbol{x}_i(t) + \boldsymbol{B}u_i(t) + \boldsymbol{F}\boldsymbol{\delta}_i\left[\boldsymbol{C}_1\boldsymbol{x}_i(t) + \boldsymbol{C}_2 u_i(t)\right] \\ + \boldsymbol{B}_d\varepsilon_i(t) \end{aligned} \tag{8}$$

where

$$\begin{aligned} \boldsymbol{x}_i(t) &= \begin{bmatrix} p_i(t) \\ v_i(t) \\ a_i(t) \end{bmatrix}, \\ \boldsymbol{A} &= \begin{bmatrix} 0 & 1 & 0 \\ 0 & 0 & 1 \\ 0 & 0 & -c \end{bmatrix}, \\ \boldsymbol{B} &= \begin{bmatrix} 0 \\ 0 \\ b \end{bmatrix}, \\ \boldsymbol{F} &= \begin{bmatrix} 0 & 0 \\ 0 & 0 \\ 1 & 1 \end{bmatrix}, \\ \boldsymbol{C}_1 &= \begin{bmatrix} 0 & 0 & r_c \\ 0 & 0 & 0 \end{bmatrix}, \\ \boldsymbol{C}_2 &= \begin{bmatrix} 0 \\ r_b \end{bmatrix}, \\ \boldsymbol{B}_d &= \begin{bmatrix} 0 \\ 0 \\ 1 \end{bmatrix}, \\ c &= 0.5\left(\frac{1}{\tau_{\min}} + \frac{1}{\tau_{\max}}\right), \\ b &= 0.5\left(k_{\min} + k_{\max}\right), \\ r_c &= 0.5\left(\frac{1}{\tau_{\min}} - \frac{1}{\tau_{\max}}\right), \\ r_b &= 0.5\left(k_{\max} - k_{\min}\right), \\ \boldsymbol{\delta}_i &= \operatorname{diag}\left[\frac{(c - 1/\tau_i)}{r_c}, \frac{(k_i - b)}{r_b}\right]. \end{aligned} \tag{9}$$

It can be concluded from the definitions of b, c, r_b, and r_c that $\|\boldsymbol{\delta}_i\|_\infty \le 1$.

2.4. Graphical Model of Interaction Topology. To generalize a unified model for various interaction topologies, the algebraic graph technique is adopted [14]:

$$\mathscr{G}(t) = \mathscr{L}(t) + \mathscr{P}(t) \tag{10}$$

where $\mathscr{G}(t) \in \mathbb{R}^{N\times N}$ indicates the information connection among vehicles, $\mathscr{L}(t)$ is called Laplacian matrix, and $\mathscr{P}(t)$ is

the pinning matrix. $\mathscr{L}(t)$ describes the directional connection among followers:

$$\mathscr{L}(t) = \left[l_{ij}(t)\right] \in \mathbb{R}^{N\times N}$$
$$l_{ii}(t) = -\sum_{j=1, j\neq i}^{N} l_{ij}(t), \quad i = 1, \cdots, N \tag{11}$$

If follower i communicates with follower j, $l_{ij}(t) = -1$, otherwise, $l_{ij}(t) = 0$. $\mathscr{P}(t)$ represents the directional connection from leader to followers:

$$\mathscr{P}(t) = \mathrm{diag}\left[g_1(t), \cdots, g_N(t)\right] \in \mathbb{R}^{N\times N} \tag{12}$$

where diag$(\cdot)$ denotes a diagonal matrix with the function variable being its diagonal elements. If follower i communicates with leader, $g_i(t) = 1$; otherwise $g_i(t) = 0$.

Considering the fact that a platoon normally holds for a relative long time and from the view of control, the influence of cut-in/off can be considered as an initial disturbance which attenuates to zero over time; the dimension of $\mathscr{G}(t)$, i.e., the platoon length N, is assumed to be a constant. Moreover, since the propagation medium for electromagnetic wave of wireless communication is passive and linear, the communication is assumed to be bidirectional, which implies that $l_{ij}(t) = l_{ji}(t)$ leading to a symmetrical topological matrix. During the running, the wireless connection is affected by surroundings. And so essentially the interaction topology is an uncertain, but piecewise constant matrix:

$$\mathscr{G}(t) = \begin{cases} \mathscr{G}_1, & 0 \le t < t_1 \\ \mathscr{G}_2, & t_1 \le t < t_2 \\ \vdots & \end{cases} \tag{13}$$

where t_k, $k = 1, 2, \cdots$ is the time when $\mathscr{G}(t)$ changes.

2.5. Distributed State Feedback. The heterogeneous feedback structure has advantages over homogeneous one in some performances such as string stability, but only special topologies such as biodirectional can be dealt with [15]. To provide a synthesis strategy applicable for a variety of topologies and simplify the theoretical analysis, the identical state feedback control logic is used here [18, 20, 33]:

$$u_i(t) = \boldsymbol{K}\sum_{j\in\mathbb{N}_i(t)}\left\{\boldsymbol{x}_i(t) - \boldsymbol{x}_j(t) - \begin{bmatrix}(i-j)\,d_0\\ 0\\ 0\end{bmatrix}\right\} \tag{14}$$

where $\boldsymbol{K} \in \mathbb{R}^3$ is the state feedback to be designed. $\mathbb{N}_i(t)$ is the neighbor set of node i:

$$\mathbb{N}_i(t) = \begin{cases} \left\{j \mid l_{ij}(t) = -1\right\}, & \text{if } g_i(t) = 0 \\ \left\{j \mid l_{ij}(t) = -1\right\} \cup \{0\}, & \text{else} \end{cases} \tag{15}$$

The information is transferred among vehicles by wireless communication, whose time delay can be handled by selecting proper state feedback or interaction topologies [25, 26, 31]. This paper focuses on the uncertainties of node dynamics and interaction topologies, and the communication delay is not considered. The objective is to find a proper $\boldsymbol{K}$ such that the platoon system is robust stable and its performance degradation caused by disturbances $\varepsilon_i(t)$ is attenuated sufficiently in the presence of the uncertainty in both node dynamics and interaction topologies.

3. Synthesis of Distributed H_∞ Controller

Considering the control objective (1), an error signal $\boldsymbol{e}_i(t) = \boldsymbol{x}_i(t) - \boldsymbol{x}_0(t) - \left[(i-j)d_0 \;\; 0 \;\; 0\right]^{\mathrm{T}}$ is defined. Its dynamical function is obtained from (8):

$$\dot{\boldsymbol{e}}_i(t) = \boldsymbol{F}\boldsymbol{\delta}_i\boldsymbol{C}_1\boldsymbol{e}_i(t) + \boldsymbol{F}\boldsymbol{\delta}_i\boldsymbol{C}_2u_i(t) + \boldsymbol{B}_d\epsilon_i(t). \tag{16}$$

And the feedback controller (14) is rewritten as

$$u_i(t) = \boldsymbol{K}\sum_{j\in\mathbb{N}_i(t)}\left\{\boldsymbol{e}_i(t) - \boldsymbol{e}_j(t)\right\}. \tag{17}$$

Then the closed loop dynamics of platoon is derived by substituting (17) into (16) and combining all control error dynamics together with $\mathscr{G}(t)$:

$$\begin{aligned}
&\dot{\boldsymbol{E}}(t)\\
&\quad = \left[\boldsymbol{I}_N\otimes\boldsymbol{A} + \mathscr{G}(t)\otimes(\boldsymbol{B}\boldsymbol{K})\right]\boldsymbol{E}(t)\\
&\qquad + \left(\boldsymbol{I}_N\otimes\boldsymbol{F}\right)\Delta\left[\boldsymbol{I}_N\otimes\boldsymbol{C}_1 + \mathscr{G}(t)\otimes\left(\boldsymbol{C}_2\boldsymbol{K}\right)\right]\boldsymbol{E}(t)\\
&\qquad + \left(\boldsymbol{I}_N\otimes\boldsymbol{B}_d\right)\Gamma(t)\\
&\boldsymbol{E}(t) = \left[\boldsymbol{e}_1(t) \;\; \cdots \;\; \boldsymbol{e}_N(t)\right]^{\mathrm{T}}\\
&\Delta = \mathrm{diag}\left(\boldsymbol{\delta}_1, \cdots, \boldsymbol{\delta}_N\right)\\
&\Gamma(t) = \left[\epsilon_1(t) \;\; \cdots \;\; \epsilon_N(t)\right]^{\mathrm{T}}\\
&\epsilon_i(t) = \varepsilon_i(t) - \dot{a}_0(t) - \frac{a_0(t)}{\tau_i}
\end{aligned} \tag{18}$$

where symbol "⊗" denotes the Kronecker product, $\boldsymbol{I}_N \in \mathbb{R}^{N\times N}$ is the identity matrix, $\|\Delta\|_\infty \le 1$ since $\|\boldsymbol{\delta}_i\|_\infty \le 1$, and $\epsilon_i(t)$ is considered as an external disturbance arising from both leader's acceleration/deceleration and model uncertainties. Before introducing the synthesis procedure, some useful lemmas are introduced.

Lemma 1 (see [35]). *There exists the following eigenvalue decomposition for matrix $\mathscr{G} = \mathscr{G}^{\mathrm{T}} \in \mathbb{R}^{N\times N}$:*

$$\mathscr{G} = \boldsymbol{H}\Lambda\boldsymbol{H}^{-1}, \quad \Lambda = \mathrm{diag}\left(\lambda_1, \cdots, \lambda_N\right) \tag{19}$$

where λ_i is the eigenvalues of $\mathscr{G}$ and $\boldsymbol{H} \in \mathbb{R}^{N\times N}$ is an unit orthogonal matrix satisfying $\boldsymbol{H}^{\mathrm{T}} = \boldsymbol{H}^{-1}$.

Lemma 2 (see [33, 34]). *For the matrices $\boldsymbol{D}$, $\boldsymbol{F}$, and $\boldsymbol{Y} = \boldsymbol{Y}^{\mathrm{T}}$, the following inequality establishes for $\forall\Delta$ satisfying $\Delta^{\mathrm{T}}\Delta \le 1$:*

$$\boldsymbol{Y} + \boldsymbol{D}\Delta\boldsymbol{F} + (\boldsymbol{D}\Delta\boldsymbol{F})^{\mathrm{T}} < 0 \tag{20}$$

if and only if $\exists \beta > 0$ *such that*

$$\boldsymbol{Y} + \beta \boldsymbol{D}\boldsymbol{D}^{\mathrm{T}} + \beta^{-1}\boldsymbol{F}^{\mathrm{T}}\boldsymbol{F} < 0. \tag{21}$$

3.1. Decoupling of Platoon Dynamics. From (18), it can be found that the closed dynamics of platoon is influenced by both the state feedback and interaction topology. If the interaction topology is determined in advance and holds during running, many control theories can be used [15–20]. Unfortunately, both the dimension and structure of the topological matrix are uncertain in a real environment, which poses a great challenge to synthesize and analyze the platoon control system. Essentially, the platoon can be considered as a network system composed of multinodes coupling with both space and time depicted by Figure 3. To covert such a complex coupling system to traditional dynamical plants for control synthesis, the interaction of nodes should be decoupled firstly.

From Lemma 1, any time segment $[t_{k-1}, t_k)$ $\mathscr{G}_k$ has the eigenvalue decomposition:

$$\mathscr{G}_k = \boldsymbol{V}_k \boldsymbol{\Lambda}_k \boldsymbol{V}_k^{-1}, \quad \boldsymbol{\Lambda}_k = \mathrm{diag}\left(\lambda_{k1}, \cdots, \lambda_{kN}\right) \tag{22}$$

where $\boldsymbol{V}_k$ is unit orthogonal matrix. The platoon system is decoupled to the following subsystems by substituting (22) into (18) and doing linear transformation:

$$\begin{aligned}
\dot{\overline{\boldsymbol{E}}}_k(t) &= \left[\boldsymbol{I}_N \otimes \boldsymbol{A} + \boldsymbol{\Lambda}_k \otimes (\boldsymbol{B}\boldsymbol{K})\right] \overline{\boldsymbol{E}}_k(t) \\
&\quad + \left(\boldsymbol{I}_N \otimes \boldsymbol{F}\right) \overline{\boldsymbol{\Delta}}_k \left[\boldsymbol{I}_N \otimes \boldsymbol{C}_1 + \boldsymbol{\Lambda}_k \otimes \left(\boldsymbol{C}_2\boldsymbol{K}\right)\right] \overline{\boldsymbol{E}}_k(t) \\
&\quad + \left(\boldsymbol{I}_N \otimes \boldsymbol{B}_d\right) \overline{\boldsymbol{\Gamma}}_k(t) \quad t \in \left[t_{k-1}, t_k\right)
\end{aligned} \tag{23}$$

where $\overline{\boldsymbol{E}}_k(t) = (\boldsymbol{V}_k^{-1} \otimes \boldsymbol{I}_3)\boldsymbol{E}(t)$, $\overline{\boldsymbol{\Gamma}}_k(t) = (\boldsymbol{V}_k^{-1} \otimes \boldsymbol{I}_3)\boldsymbol{\Gamma}(t)$, $\overline{\boldsymbol{\Delta}}_k = (\boldsymbol{V}_k^{-1} \otimes \boldsymbol{I}_3)\boldsymbol{\Delta}(\boldsymbol{V}_k \otimes \boldsymbol{I}_3)$.

It can be found that in the spatial domain (23) is almost a diagonal system besides the coupling of $\overline{\boldsymbol{\Delta}}$, and in the time domain the dynamics of decoupled platoon is connected by multiple time-invariant system with uncertainties. Furthermore, though the linear transformation is different in different time segments, the amplitude of signals and the $\boldsymbol{H}_\infty$ norm of uncertainty remain unchanged because $\boldsymbol{V}_k^{\mathrm{T}}\boldsymbol{V}_k = \boldsymbol{I}_N$:

$$\begin{aligned}
\left|\overline{\boldsymbol{E}}_k(t)\right| &= \left|\boldsymbol{E}(t)\right|, \\
\left|\overline{\boldsymbol{\Gamma}}_k(t)\right| &= \left|\boldsymbol{\Gamma}(t)\right| \\
\left\|\overline{\boldsymbol{\Delta}}_k\right\|_\infty &= \left\|\boldsymbol{\Delta}\right\|_\infty
\end{aligned} \tag{24}$$

where $|\cdot|$ is the $\mathbf{L}_2$ norm of a signal and its induced norm is $\|\cdot\|_\infty$. The following theorem converts the problem of $\boldsymbol{H}_\infty$ performance into the existence of multiple inequalities by using the invariance property of signal amplitude of the aforementioned linear transformation.

Theorem 3. *If* $\exists \boldsymbol{P}^{\mathrm{T}} = \boldsymbol{P} > 0 \in \mathbb{R}^{3\times 3}$ *such that*

$$\begin{bmatrix} \boldsymbol{M}_{1k}^{\mathrm{T}} + \boldsymbol{M}_{1k} + \boldsymbol{M}_3\overline{\boldsymbol{\Delta}}_k\boldsymbol{M}_{2k} + \boldsymbol{M}_{2k}^{\mathrm{T}}\overline{\boldsymbol{\Delta}}_k^{\mathrm{T}}\boldsymbol{M}_3^{\mathrm{T}} + \boldsymbol{I}_N \otimes \left(\boldsymbol{Q}^{\mathrm{T}}\boldsymbol{Q}\right) & \boldsymbol{I}_N \otimes (\boldsymbol{P}\boldsymbol{B}_d) \\ * & -\gamma^2 \end{bmatrix} < 0, \quad k = 1, 2, \cdots$$

$$\begin{aligned}
\boldsymbol{M}_{1k} &= \boldsymbol{I}_N \otimes (\boldsymbol{P}\boldsymbol{A}) + \boldsymbol{\Lambda}_k \otimes (\boldsymbol{P}\boldsymbol{B}\boldsymbol{K}) \\
\boldsymbol{M}_{2k} &= \boldsymbol{I}_N \otimes \boldsymbol{C}_1 + \boldsymbol{\Lambda}_k \otimes \left(\boldsymbol{C}_2\boldsymbol{K}\right) \\
\boldsymbol{M}_3 &= \boldsymbol{I}_N \otimes (\boldsymbol{P}\boldsymbol{F})
\end{aligned} \tag{25}$$

where "$*$*" denotes the symmetrical part, then the closed loop platoon system (18) is as follows:*

(C1) asymptotically stable;

(C2) with the zero initial state and weighting matrix $\boldsymbol{Q} \in \mathbb{R}^{3\times 3}$*, the disturbance* $\boldsymbol{\Gamma}(t)$ *is attenuated by*

$$\left\|\left(\boldsymbol{I}_N \otimes \boldsymbol{Q}\right)\boldsymbol{E}(t)\right\|_2 < \gamma \left\|\boldsymbol{\Gamma}(t)\right\|_2. \tag{26}$$

Proof. By applying the Schur Complement Theorem to (21), the following inequality establishes for $\forall k = 1, 2, \cdots$:

$$\begin{aligned}
&\boldsymbol{M}_{1k}^{\mathrm{T}} + \boldsymbol{M}_{1k} + \boldsymbol{M}_3\overline{\boldsymbol{\Delta}}_k\boldsymbol{M}_{2k} + \boldsymbol{M}_{2k}^{\mathrm{T}}\overline{\boldsymbol{\Delta}}_k^{\mathrm{T}}\boldsymbol{M}_3^{\mathrm{T}} \\
&< -\boldsymbol{I}_N \otimes \left(\boldsymbol{Q}^{\mathrm{T}}\boldsymbol{Q}\right) < 0
\end{aligned} \tag{27}$$

Then defining the following Lyapuonv function and considering (24), at $\forall t \in [t_{k-1}, t_k)$ we have

$$L(t) = \boldsymbol{E}^{\mathrm{T}}(t)\left(\boldsymbol{I}_N \otimes \boldsymbol{P}\right)\boldsymbol{E}(t) = \overline{\boldsymbol{E}}_k^{\mathrm{T}}(t)\left(\boldsymbol{I}_N \otimes \boldsymbol{P}\right)\overline{\boldsymbol{E}}_k(t). \tag{28}$$

Substituting (23) into the time derivation of $L(t)$ yields

$$\begin{aligned}
\dot{L}(t) &= \overline{\boldsymbol{E}}_k^{\mathrm{T}}(t) \\
&\quad \cdot \left(\boldsymbol{M}_{1k}^{\mathrm{T}} + \boldsymbol{M}_{1k} + \boldsymbol{M}_3\overline{\boldsymbol{\Delta}}_k\boldsymbol{M}_{2k} + \boldsymbol{M}_{2k}^{\mathrm{T}}\overline{\boldsymbol{\Delta}}_k^{\mathrm{T}}\boldsymbol{M}_3^{\mathrm{T}}\right) \\
&\quad \cdot \overline{\boldsymbol{E}}_k(t).
\end{aligned} \tag{29}$$

We can found that $\dot{L}(t) < 0$, if $\boldsymbol{E}(t) \neq 0$ by substituting (27) into (29). From the Lyapunov theory it is known that (18) is asymptotically stable and conclusion (C1) is proved.

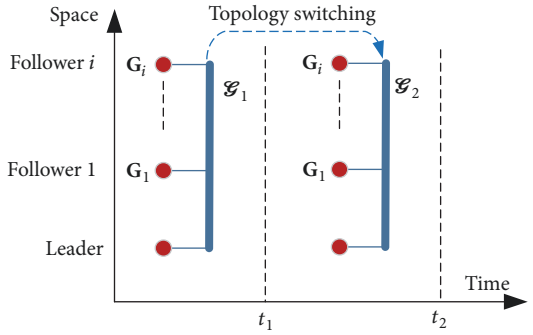

FIGURE 3: Spatial and time coupling of nodes.

During any time segment $[t_{k-1}, t_k)$, we have

$$\begin{aligned} J_k &= \int_{t_{k-1}}^{t_k} \left[\left| (\boldsymbol{I}_N \otimes \boldsymbol{Q}) \, \overline{\boldsymbol{E}}_k(\tau) \right|^2 - \gamma^2 \left| \overline{\boldsymbol{\Gamma}}_k(t) \right|^2 \right] \mathrm{d}\tau \\ &= \int_{t_{k-1}}^{t_k} \left[\left| (\boldsymbol{I}_N \otimes \boldsymbol{Q}) \, \overline{\boldsymbol{E}}_k(\tau) \right|^2 - \gamma^2 \left| \overline{\boldsymbol{\Gamma}}_k(t) \right|^2 \right. \\ &\quad \left. + \frac{\mathrm{d}L(\tau)}{\mathrm{d}\tau} \right] \mathrm{d}\tau + L(t_{k-1}) - L(t_k). \end{aligned} \tag{30}$$

Substituting (25) and (29) into (30) yields

$$J_k < L(t_{k-1}) - L(t_k). \tag{31}$$

Then from (28) and (31) we have the following inequality and conclusion (C2) is proved:

$$\begin{aligned} \left\| (\boldsymbol{I}_N \otimes \boldsymbol{Q}) \, \boldsymbol{E}(t) \right\|_2^2 - \gamma^2 \left\| \boldsymbol{\Gamma}(t) \right\|_2^2 &= \sum_{k=1,2,\cdots} J_k \\ < \sum_{k=1,2,\cdots} L(t_{k-1}) - L(t_k) &= L(0) - L(t) < 0 \end{aligned} \tag{32}$$

□

Theorem 3 provides a sufficient condition for the robust performance of platoon. The existence of required $\boldsymbol{P}$ depends on $\boldsymbol{\Lambda}_k$ and the attenuation ability. There is maybe no solution if the requirement of attenuation is too high. And for the nonscalable platoon, the minimum eigenvalue of topology tends to zero with the increasing of platoon length. From (23), the mode corresponding to the zero eigenvalue becomes uncontrollable. This implies that the length of nonscalable platoon is limited; otherwise its robust performance may not be ensured. Moreover for platooning string stability is an important property. When using the state feedback control strategy, the leader information is necessary to ensure it [2]. Here, the information connection between vehicles is uncertain. Though the string stability cannot be ensured, the average tracking error will not increase with the platoon length and is bounded by

$$\begin{aligned} \mathrm{RMS}\left[(\boldsymbol{I}_N \otimes \boldsymbol{Q}) \, \boldsymbol{E}(t) \right] &= \sqrt{\sum_{i=1}^{N} \frac{\left\| \boldsymbol{Q} \boldsymbol{e}_i(t) \right\|_2^2}{N}} \\ &< \gamma \max_i \left\| \epsilon_i(t) \right\|_2. \end{aligned} \tag{33}$$

3.2. Solving the Distributed $\boldsymbol{H}_\infty$ Controller Numerically. The state feedback cannot be derived by Theorem 3 directly because of the following. (a) There are unknown parameters in (23), such as $\overline{\boldsymbol{\Delta}}_k$ and $\boldsymbol{\Lambda}_k$. (b) Equation (23) is a nonlinear function of variables $\boldsymbol{P}$ and $\boldsymbol{K}$. The following theorem provides a way to numerically solve the $\boldsymbol{H}_\infty$ controller by using the LMI method.

Theorem 4. *For $\forall \lambda_{ki} \in \left[\underline{\lambda} \;\; \overline{\lambda} \right]$ and $\|\overline{\boldsymbol{\Delta}}_k\|_\infty < 1$, (25) in Theorem 3 it is established that if and only if $\exists \overline{\boldsymbol{P}}^{\mathrm{T}} = \overline{\boldsymbol{P}} > 0 \in \mathbb{R}^{3\times 3}$, $\boldsymbol{W} \in \mathbb{R}^3$ and $\beta > 0 \in \mathbb{R}$ such that*

$$\begin{aligned} &\mathscr{F}(\underline{\lambda}) < 0 \\ &\textit{and } \mathscr{F}(\overline{\lambda}) < 0 \end{aligned}$$

$$\mathscr{F}(\lambda) = \begin{bmatrix} \boldsymbol{A}\overline{\boldsymbol{P}} + \overline{\boldsymbol{P}}\boldsymbol{A}^{\mathrm{T}} + \lambda \boldsymbol{B}\boldsymbol{W} + \lambda (\boldsymbol{B}\boldsymbol{W})^{\mathrm{T}} & \overline{\boldsymbol{P}}\boldsymbol{Q}^{\mathrm{T}} & \boldsymbol{B}_d & \boldsymbol{F} & \overline{\boldsymbol{P}}\boldsymbol{C}_1^{\mathrm{T}} + \lambda \boldsymbol{W}^{\mathrm{T}}\boldsymbol{C}_2^{\mathrm{T}} \\ * & -\boldsymbol{I} & \boldsymbol{0} & \boldsymbol{0} & \boldsymbol{0} \\ * & * & -\gamma \boldsymbol{I} & \boldsymbol{0} & \boldsymbol{0} \\ * & * & * & -\beta^{-1}\boldsymbol{I} & \boldsymbol{0} \\ * & * & * & * & -\beta \boldsymbol{I} \end{bmatrix} \tag{34}$$

Proof. Equation (25) is equivalent to the following inequality by applying the Schur Complement Theorem to (25) and then substituting $\overline{\boldsymbol{P}} = \boldsymbol{P}^{-1}, \boldsymbol{W} = \boldsymbol{K}\overline{\boldsymbol{P}}$ to it:

$$\begin{aligned} &\boldsymbol{I}_N \otimes \left(\boldsymbol{A}\overline{\boldsymbol{P}} + \overline{\boldsymbol{P}}\boldsymbol{A}^{\mathrm{T}} \right) + \boldsymbol{\Lambda}_k \otimes \left[\boldsymbol{B}\boldsymbol{W} + (\boldsymbol{B}\boldsymbol{W})^{\mathrm{T}} \right] \\ &\quad + \left[\boldsymbol{I}_N \otimes \boldsymbol{F} \right] \overline{\boldsymbol{\Delta}}_k \left[\boldsymbol{I}_N \otimes \boldsymbol{C}_1\overline{\boldsymbol{P}} + \boldsymbol{\Lambda}_k \otimes (\boldsymbol{C}_2\boldsymbol{W}) \right] \\ &\quad + \left[\boldsymbol{I}_N \otimes \boldsymbol{C}_1\overline{\boldsymbol{P}} + \boldsymbol{\Lambda}_k \otimes (\boldsymbol{C}_2\boldsymbol{W}) \right]^{\mathrm{T}} \overline{\boldsymbol{\Delta}}_k^{\mathrm{T}} \left[\boldsymbol{I}_N \otimes \boldsymbol{F} \right]^{\mathrm{T}} \\ &\quad + \boldsymbol{I}_N \otimes \left(\overline{\boldsymbol{P}}\boldsymbol{Q}^{\mathrm{T}}\boldsymbol{Q}\overline{\boldsymbol{P}} \right) + \gamma^{-2} \left[\boldsymbol{I}_N \otimes \left(\boldsymbol{B}_d\boldsymbol{B}_d^{\mathrm{T}} \right) \right] < \boldsymbol{0} \end{aligned} \tag{35}$$

From Lemma 2, (35) establishes for $\forall \|\overline{\boldsymbol{\Delta}}_k\|_\infty < 1$ if and only if $\exists \beta > 0$ such that

$$
\begin{aligned}
&\boldsymbol{I}_N \otimes \boldsymbol{M}_4 + \boldsymbol{\mathcal{F}}_1\left(\boldsymbol{\Lambda}_k\right) < \boldsymbol{0}, \quad k = 1, 2, \cdots \\
&\boldsymbol{M}_4 = \boldsymbol{A}\overline{\boldsymbol{P}} + \overline{\boldsymbol{P}}\boldsymbol{A}^{\mathrm{T}} + \overline{\boldsymbol{P}}\boldsymbol{Q}^{\mathrm{T}}\boldsymbol{Q}\overline{\boldsymbol{P}} + \gamma^{-2}\boldsymbol{B}_d\boldsymbol{B}_d^{\mathrm{T}} + \beta\boldsymbol{F}\boldsymbol{F}^{\mathrm{T}} \\
&\boldsymbol{\mathcal{F}}_1\left(\boldsymbol{\Lambda}_k\right) = \boldsymbol{\Lambda}_k \otimes \left[\boldsymbol{B}\boldsymbol{W} + (\boldsymbol{B}\boldsymbol{W})^{\mathrm{T}}\right] \\
&\quad + \beta^{-1}\left[\boldsymbol{I}_N \otimes \boldsymbol{C}_1\overline{\boldsymbol{P}} + \boldsymbol{\Lambda}_k \otimes (\boldsymbol{C}_2\boldsymbol{W})\right]^{\mathrm{T}} \\
&\quad \cdot \left[\boldsymbol{I}_N \otimes \boldsymbol{C}_1\overline{\boldsymbol{P}} + \boldsymbol{\Lambda}_k \otimes (\boldsymbol{C}_2\boldsymbol{W})\right]
\end{aligned} \tag{36}
$$

Since the left side of (36) is a block diagonal matrix, it is established if and only if

$$
\boldsymbol{M}_4 + \boldsymbol{\mathcal{F}}_1\left(\lambda_{ki}\right) < \boldsymbol{0}, \quad k = 1, 2, \cdots, \; i = 1, \cdots N. \tag{37}
$$

The necessary condition can be proved by substituting $\lambda_{ki} = \underline{\lambda}$ and $\lambda_{ki} = \overline{\lambda}$ to (37), respectively, and then applying he Schur Complement Theorem to it. Next the sufficient condition is to be proved. For $\forall\lambda_{ki} \in \left[\underline{\lambda} \;\; \overline{\lambda}\right]$ and vector $\boldsymbol{y} \in \mathbb{R}^3$ we have

$$
\begin{aligned}
\boldsymbol{y}^{\mathrm{T}}\boldsymbol{\mathcal{F}}_1\left(\lambda_{ki}\right)\boldsymbol{y} &= \left(\beta^{-1}\boldsymbol{y}^{\mathrm{T}}\boldsymbol{W}^{\mathrm{T}}\boldsymbol{C}_2^{\mathrm{T}}\boldsymbol{C}_2\boldsymbol{W}\boldsymbol{y}\right)\lambda_{ki}^2 + \boldsymbol{y}^{\mathrm{T}}\left[\boldsymbol{B}\boldsymbol{W}\right. \\
&\quad \left. + (\boldsymbol{B}\boldsymbol{W})^{\mathrm{T}} + \beta^{-1}\overline{\boldsymbol{P}}\boldsymbol{C}_1^{\mathrm{T}}\boldsymbol{C}_2\boldsymbol{W} + \beta^{-1}\boldsymbol{W}^{\mathrm{T}}\boldsymbol{C}_2^{\mathrm{T}}\boldsymbol{C}_1\overline{\boldsymbol{P}}\right]\boldsymbol{y}\lambda_{ki} \\
&\quad + \boldsymbol{y}^{\mathrm{T}}\boldsymbol{M}_4\boldsymbol{y}.
\end{aligned} \tag{38}
$$

When $\boldsymbol{y}$ is given, $\boldsymbol{y}^{\mathrm{T}}\boldsymbol{\mathcal{F}}_1(\lambda_{ki})\boldsymbol{y}$ is a quadratic function of λ_{ki}. Furthermore since $\beta^{-1}\boldsymbol{y}^{\mathrm{T}}\boldsymbol{W}^{\mathrm{T}}\boldsymbol{C}_2^{\mathrm{T}}\boldsymbol{C}_2\boldsymbol{W}\boldsymbol{y} \geq 0$ the following inequality can be derived:

$$
\boldsymbol{y}^{\mathrm{T}}\boldsymbol{\mathcal{F}}_1\left(\lambda_{ki}\right)\boldsymbol{y} \leq \max\left(\boldsymbol{y}^{\mathrm{T}}\boldsymbol{\mathcal{F}}_1\left(\underline{\lambda}\right)\boldsymbol{y}, \boldsymbol{y}^{\mathrm{T}}\boldsymbol{\mathcal{F}}_1\left(\overline{\lambda}\right)\boldsymbol{y}\right) \tag{39}
$$

On the other hand, applying the Schur Complement Theorem to (34), we have

$$
\begin{aligned}
\boldsymbol{y}^{\mathrm{T}}\left[\boldsymbol{M}_4 + \boldsymbol{\mathcal{F}}_1\left(\underline{\lambda}\right)\right]\boldsymbol{y} < 0 \\
\boldsymbol{y}^{\mathrm{T}}\left[\boldsymbol{M}_4 + \boldsymbol{\mathcal{F}}_1\left(\overline{\lambda}\right)\right]\boldsymbol{y} < 0
\end{aligned} \tag{40}
$$

Then for $\forall\lambda_{ki} \in \left[\underline{\lambda} \;\; \overline{\lambda}\right]$ combining (39) and (40) yields

$$
\boldsymbol{y}^{\mathrm{T}}\left[\boldsymbol{M}_4 + \boldsymbol{\mathcal{F}}_1\left(\lambda_{ki}\right)\right]\boldsymbol{y} < \boldsymbol{0}. \tag{41}
$$

According to the definition of negative matrix, (37) establishes and the sufficient condition is proved. □

Equation (34) is a standard LMI, which can be solved and optimized numerically. From Theorem 4, the exact eigenvalues and structure of topological matrix are not necessary and the distributed $\boldsymbol{H}_\infty$ controller can be solved and optimized numerically with only the limits of eigenvalues. There are already some methods to estimate the range of matrix eigenvalue such as the Gerschgorin Disk Theory [14].

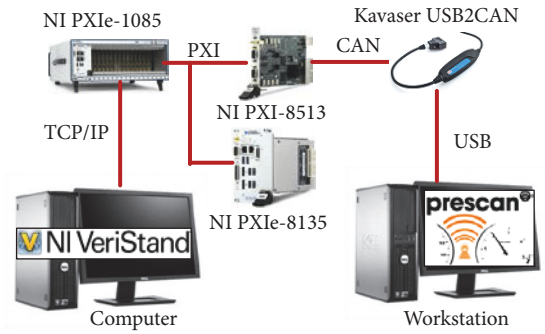

Figure 4: Bench test system for validation of the platoon control system.

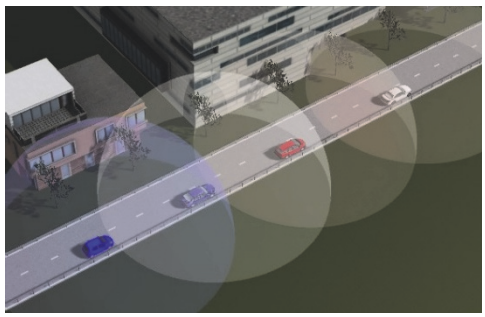

Figure 5: Virtual scenario of platoon driving in Prescan.

4. Bench Test Validation

The effectiveness of the proposed distributed $\boldsymbol{H}_\infty$ control method for platoon is validated by bench tests. The test bench is depicted by Figure 4, including a real time simulator and a VR (Virtual Reality) simulation platform [36].

The PXI platform is used to run the nonlinear vehicle dynamical models (2)~(5), the inverse models (6), and the distributed $\boldsymbol{H}_\infty$ controller in real time. The VeriStand is used to manage this simulator. Each vehicle is equipped with a V2V equipment. The scenarios and wireless communication are modeled in Prescan (See Figure 5), which is a real time VR simulation platform for AV. The signals of the PXI platform and Prescan are exchanged by CAN (Control Area Network) [37].

4.1. Test Conditions. The tested platoon is composed of one leader and 20 followers. The desired distance between two neighboring vehicles is 5 m. The leader runs according to a naturalistic acceleration/velocity profile, which is from the driver experiment data and shown in Figure 6.

A statistical model is used to describe the success possibility $P_{i,j}$ of a packet delivery between two communicating vehicles [12]:

$$
\begin{aligned}
P_{ij} &= \begin{cases} \rho_{ij}, & \text{if } \rho_{ij} > 0 \\ 0, & \text{otherwise,} \end{cases} \\
\rho_{ij} &= -\frac{1}{400}\left|p_i - p_j\right|^2 + 100.
\end{aligned} \tag{42}
$$

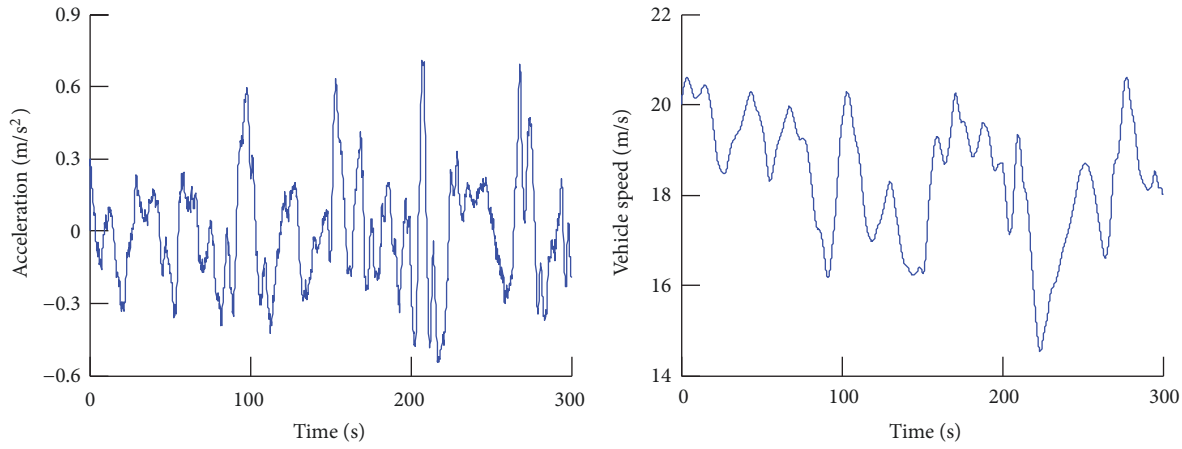

(a) Acceleration (b) Vehicle speed

Figure 6: Profiles of the lead vehicle.

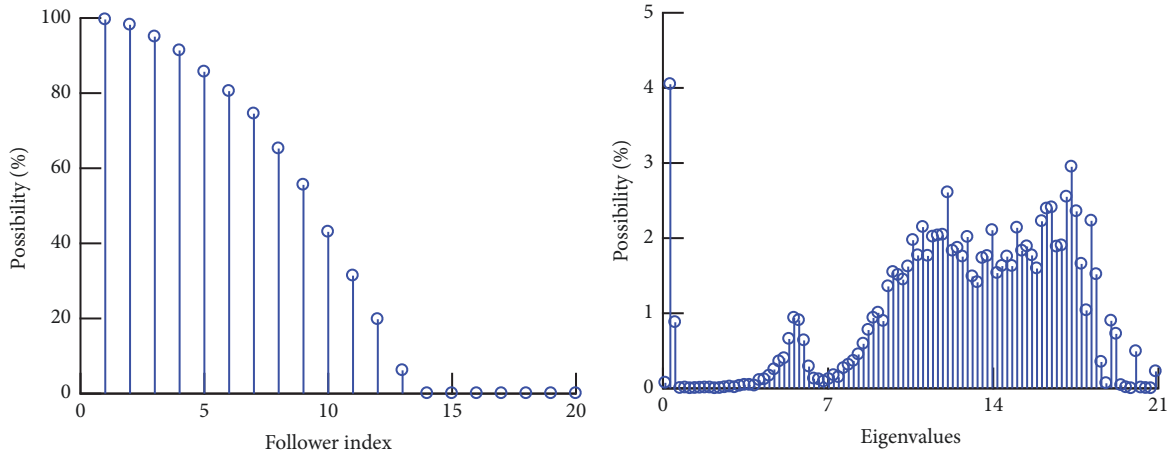

(a) Possibility of successful connection (b) Distribution of eigenvalues

Figure 7: Statistical results of communication.

4.2. Results under Nominal Condition. Firstly, tests were conducted under the nominal condition that all parameters of followers are set to their nominal values (see Table 1) and there is no environmental disturbances. The results are shown in Figures 7 and 8.

Figure 7(a) shows the success possibility of a packet delivery between leader and followers, which is coincident with the statistical model described by (42). When the vehicles in the platoon are coupled by such random information connections. The distribution of topological eigenvalues is shown in Figure 7(b), from which it can be found that the value varies in a large range. Figure 8 is the tracking errors and to show clearly, only the maximum and minimum ones are presented here. From these results, the maximum tracking errors of position and speed are 0.6 m and 0.2 m/s, respectively. All followers have a high degree of uniformity with regard to the following behavior, because of the homogeneity of platoon.

4.3. Robust Performance. To further validate the effectiveness of the proposed distributed $\boldsymbol{H}_\infty$ controller, periodical external disturbances arising from wind and road slope (shown in Figure 9) are added during bench testing.

Moreover the uncertain vehicle parameters are selected randomly from their possible ranges (see Table 1) before simulation, which leads to an uncertain and heterogeneous platoon. Figure 10 shows the results under this nonideal condition. The maximum tracking errors of position and speed are 0.7 m and 0.35 m/s, respectively. Comparing with the nominal condition, the tracking errors increase only a little, which implies that this $\boldsymbol{H}_\infty$ controller successfully attenuates the disturbances arising from external resistances, uncertain vehicle parameters, and randomly switching topology. And because of the heterogeneity of platoon, the following behavior of each follower becomes different.

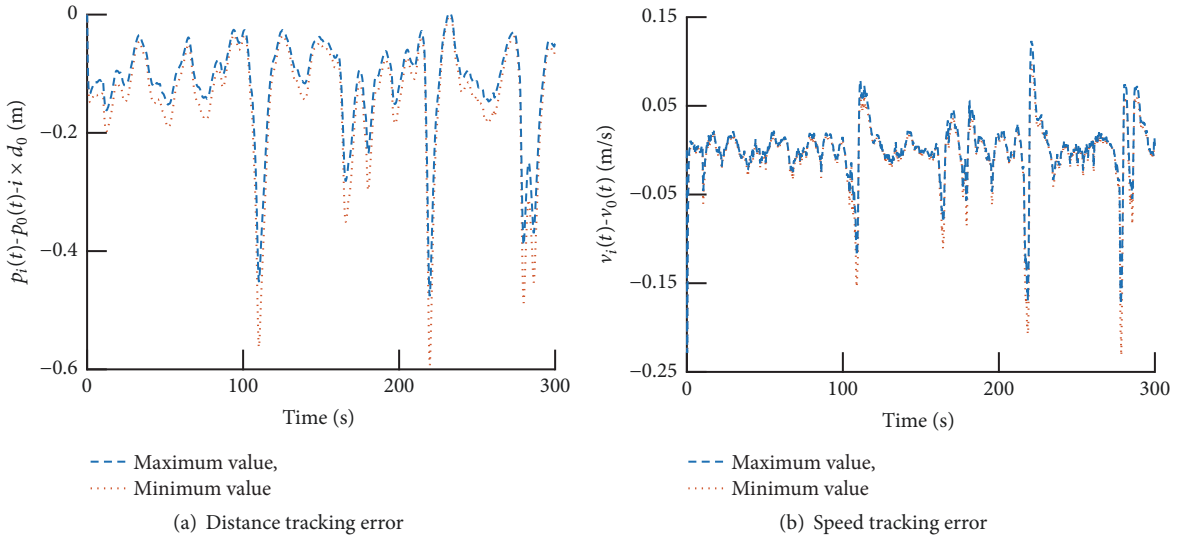

(a) Distance tracking error (b) Speed tracking error

Figure 8: Maximum and minimum tracking errors under the nominal condition.

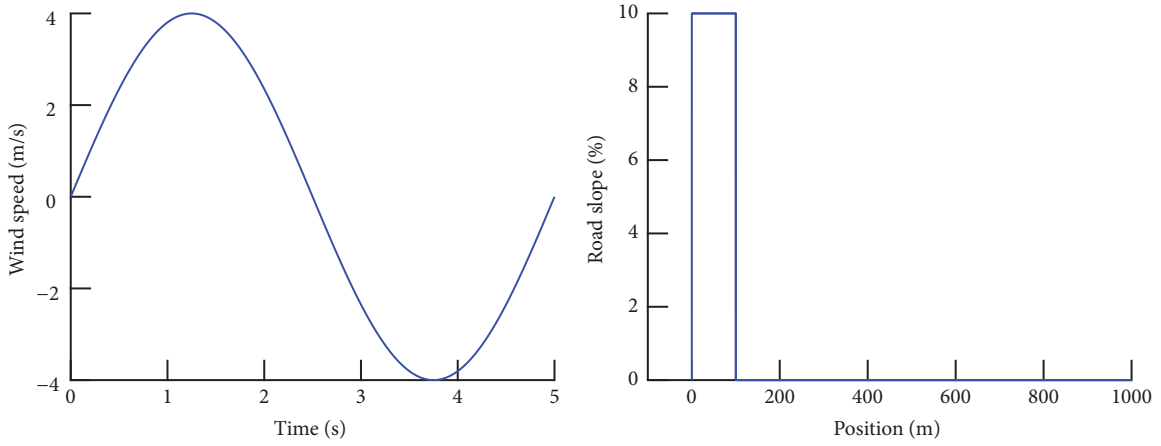

(a) Wind speed (b) Road slope

Figure 9: One period of external resistances.

To further validate the effectiveness of the proposed method, it has been compared with a nonrobust state feedback $\boldsymbol{K} = [-8 \ -8 \ -1]$, which only considers the stability region [14]. The results are shown in Figure 11, from which it is found that the maximum distance and speed tracking errors of nonrobust controller are more than 1.6 m and 1.2 m/s, and they are almost twice the robust one.

5. Conclusion

This paper presents a distributed $\boldsymbol{H}_\infty$ control method for platoon with uncertain node dynamics and interaction topologies. The following conclusions are obtained from the theoretical analysis and bench tests:

(1) It is necessary to consider the uncertainty of vehicle dynamics, external disturbances, and nonideal characteristic of wireless communication when synthesizing a vehicular platoon system.

(2) The proposed distributed $\boldsymbol{H}_\infty$ controller can ensure the robust stability and tracking performance of a platoon in the presence of uncertainties in both vehicle dynamics and interaction topology.

Data Availability

The node dynamical model and its excitation and response data used to model the uncertain linear node dynamics are available from the corresponding author upon request. The

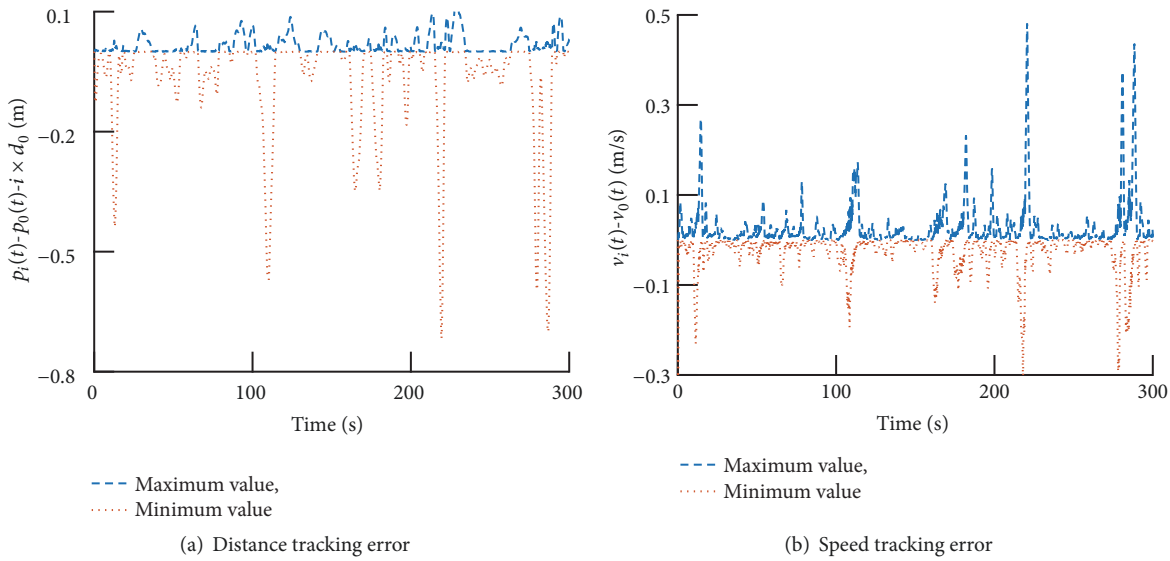

(a) Distance tracking error (b) Speed tracking error

Figure 10: Maximum and minimum tracking errors under the disturbed condition.

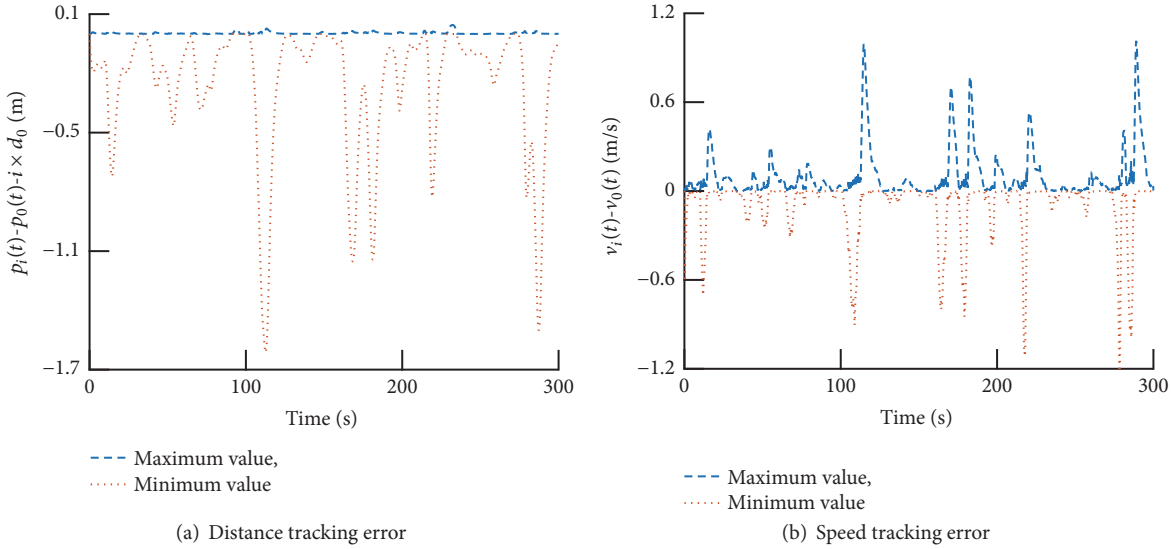

(a) Distance tracking error (b) Speed tracking error

Figure 11: Simulation results of nonrobust controller.

simulation model of platooning and the simulated results used to support the findings of this study are available from the corresponding author upon request.

Conflicts of Interest

The authors declare that they have no conflicts of interest.

Acknowledgments

This research is supported by National key research and development program under Grants 2016YFB0100900, 2016YFB0101104, and 2017YFB0102504 and Open fund of State Key Laboratory of Vehicle NVH and Safety Technology under Grant NVHSKL-201705.

References

[1] Y. Wiseman, "Autonomous vehicles," in *Encyclopedia of Organizational Knowledge, Administration, and Technologies*, 1st edition, 2019.

[2] S. E. Shladover, C. A. Desoer, J. K. Hedrick et al., "Automated vehicle control developments in the PATH program," *IEEE Transactions on Vehicular Technology*, vol. 40, no. 1, pp. 114–130, 1991.

[3] J. Zhang, F.-Y. Wang, K. Wang, W.-H. Lin, X. Xu, and C. Chen, "Data-driven intelligent transportation systems: a survey," *IEEE Transactions on Intelligent Transportation Systems*, vol. 12, no. 4, pp. 1624–1639, 2011.

[4] E. Chan, P. Gilhead, P. Jelinek, P. Krejci, and T. Robinson, "Cooperative control of SARTRE automated platoon vehicles," in *Proceedings of the 19th Intelligent Transport Systems World Congress, ITS 2012*, pp. 1–9, Vienna, Austria, 2012.

[5] S. E. Li, F. Gao, D. Cao, and K. Li, "Multiple-model switching control of vehicle longitudinal dynamics for platoon-level automation," *IEEE Transactions on Vehicular Technology*, vol. 65, no. 6, pp. 4480–4492, 2016.

[6] D. Swaroop, J. K. Hedrick, C. C. Chien, and P. Ioannou, "A comparision of spacing and headway control laws for automatically controlled vehicles," *Vehicle System Dynamics*, vol. 23, no. 8, pp. 597–625, 1994.

[7] D. Swaroop and J. K. Hedrick, "Constant spacing strategies for platooning in automated highway systems," *Journal of Dynamic Systems, Measurement, and Control*, vol. 121, no. 3, pp. 462–470, 1999.

[8] E. Shaw and J. K. Hedrick, "String stability analysis for heterogeneous vehicle strings," in *Proceedings of the 2007 American Control Conference, ACC*, pp. 3118–3125, New York, NY, USA, 2007.

[9] L. Xiao and F. Gao, "Practical string stability of platoon of adaptive cruise control vehicles," *IEEE Transactions on Intelligent Transportation Systems*, vol. 12, no. 4, pp. 1184–1194, 2011.

[10] C.-Y. Liang and H. Peng, "Optimal adaptive cruise control with guaranteed string stability," *Vehicle System Dynamics*, vol. 32, no. 4, pp. 313–330, 1999.

[11] Z. Wang, G. Wu, and M. J. Barth, "Developing a distributed consensus-based cooperative adaptive cruise control system for heterogeneous vehicles with predecessor following topology," *Journal of Advanced Transportation*, vol. 2017, Article ID 1023654, 16 pages, 2017.

[12] K. Li, F. Gao, S. E. Li, Y. Zheng, and H. Gao, "Robust cooperation of connected vehicle systems with eigenvalue-bounded interaction topologies in the presence of uncertain dynamics," *Frontiers of Mechanical Engineering*, vol. 13, no. 3, pp. 354–367, 2018.

[13] T. Willke, P. Tientrakool, and N. Maxemchuk, "A survey of inter-vehicle communication protocols and their applications," *IEEE Communications Surveys & Tutorials*, vol. 11, no. 2, pp. 3–20, 2009.

[14] Y. Zheng, S. E. Li, J. Wang, D. Cao, and K. Li, "Stability and scalability of homogeneous vehicular platoon: study on the influence of information flow topologies," *IEEE Transactions on Intelligent Transportation Systems*, vol. 17, no. 1, pp. 14–26, 2016.

[15] A. Ghasemi, R. Kazemi, and S. Azadi, "Stable decentralized control of a platoon of vehicles with heterogeneous information feedback," *IEEE Transactions on Vehicular Technology*, vol. 62, no. 9, pp. 4299–4308, 2013.

[16] Y. Zheng, S. E. Li, K. Li, and L.-Y. Wang, "Stability margin improvement of vehicular platoon considering undirected topology and asymmetric control," *IEEE Transactions on Control Systems Technology*, vol. 24, no. 4, pp. 1253–1265, 2016.

[17] K. Raghuwaiya, B. Sharma, and J. Vanualailai, "Leader-follower based locally rigid formation control," *Journal of Advanced Transportation*, vol. 2018, Article ID 5278565, 14 pages, 2018.

[18] J. Wang, Z. Duan, G. Wen, and G. Chen, "Distributed robust control of uncertain linear multiagent systems," *International Journal of Robust and Nonlinear Control*, vol. 25, no. 13, pp. 2162–2179, 2015.

[19] F. Gao, D. F. Dang, S. S. Huang, and S. E. Li, "Decoupled robust control of vehicular platoon with identical controller and rigid information flow," *International Journal of Automotive Technology*, vol. 18, no. 1, pp. 157–164, 2017.

[20] Q. Xia, F. Gao, J. Duan, and Y. He, "Decoupled H∞ control of automated vehicular platoons with complex interaction topologies," *IET Intelligent Transport Systems*, vol. 11, no. 2, pp. 92–101, 2017.

[21] M. Yan, Y. Tang, P. Yang, and L. Zuo, "Consensus based platoon algorithm for velocity-measurement-absent vehicles with actuator saturation," *Journal of Advanced Transportation*, vol. 2017, Article ID 8023018, 8 pages, 2017.

[22] J.-W. Kwon and D. Chwa, "Adaptive bidirectional platoon control using a coupled sliding mode control method," *IEEE Transactions on Intelligent Transportation Systems*, vol. 15, no. 5, pp. 2040–2048, 2014.

[23] R. Li, L. Zhang, L. Han, and J. Wang, "Multiple vehicle formation control based on robust adaptive control algorithm," *IEEE Intelligent Transportation Systems Magazine*, vol. 9, no. 2, pp. 41–51, 2017.

[24] R. Teo, D. M. Stipanović, and C. J. Tomlin, "Decentralized spacing control of a string of multiple vehicles over lossy datalinks," *IEEE Transactions on Control Systems Technology*, vol. 18, no. 2, pp. 469–473, 2010.

[25] L. Y. Wang, A. Syed, G. G. Yin, A. Pandya, and H. Zhang, "Control of vehicle platoons for highway safety and efficient utility: consensus with communications and vehicle dynamics," *Journal of Systems Science and Complexity*, vol. 27, no. 4, pp. 605–631, 2014.

[26] F. Gao, S. E. Li, Y. Zheng, and D. Kum, "Robust control of heterogeneous vehicular platoon with uncertain dynamics and communication delay," *IET Intelligent Transport Systems*, vol. 10, no. 7, pp. 503–513, 2016.

[27] F. Gao, X. Hu, S. E. Li, K. Li, and Q. Sun, "Distributed adaptive sliding mode control of vehicular platoon with uncertain interaction topology," *IEEE Transactions on Industrial Electronics*, vol. 65, no. 8, pp. 6352–6361, 2018.

[28] G. Wen, G. Hu, W. Yu, J. Cao, and G. Chen, "Consensus tracking for higher-order multi-agent systems with switching directed topologies and occasionally missing control inputs," *Systems & Control Letters*, vol. 62, no. 12, pp. 1151–1158, 2013.

[29] N. Chen, M. Wang, T. Alkim, and B. van Arem, "A robust longitudinal control strategy of platoons under model uncertainties and time delays," *Journal of Advanced Transportation*, vol. 2018, Article ID 9852721, 13 pages, 2018.

[30] M. Di Bernardo, A. Salvi, and S. Santini, "Distributed consensus strategy for platooning of vehicles in the presence of time-varying heterogeneous communication delays," *IEEE Transactions on Intelligent Transportation Systems*, vol. 16, no. 1, pp. 102–112, 2015.

[31] M. Di Bernardo, P. Falcone, A. Salvi, and S. Santini, "Design, analysis, and experimental validation of a distributed protocol for platooning in the presence of time-varying heterogeneous delays," *IEEE Transactions on Control Systems Technology*, vol. 24, no. 2, pp. 413–427, 2016.

[32] K. Massow and I. Radusch, "A rapid prototyping environment for cooperative advanced driver assistance systems," *Journal of Advanced Transportation*, vol. 2018, Article ID 2586520, 32 pages, 2018.

[33] F. Gao, D. Dang, S. E. Li, and M. Zhou, "Control of large model mismatch systems using multiple models," *International Journal of Control, Automation, and Systems*, vol. 15, no. 4, pp. 1494–1506, 2017.

[34] F. Gao, S. E. Li, D. Kum, and H. Zhang, "Synthesis of multiple model switching controllers using H∞ theory for systems with large uncertainties," *Neurocomputing*, vol. 157, pp. 118–124, 2015.

[35] Z. Li, Z. Duan, L. Xie, and X. Liu, "Distributed robust control of linear multi-agent systems with parameter uncertainties," *International Journal of Control*, vol. 85, no. 8, pp. 1039–1050, 2012.

[36] Q. Xia, J. Duan, F. Gao, Q. Hu, and Y. He, "Test scenario design for intelligent driving system ensuring coverage and effectiveness," *International Journal of Automotive Technology*, vol. 19, no. 4, pp. 751–758, 2018.

[37] F. Gao, J. Duan, Y. He, and Z. Wang, "A test scenario automatic generation strategy for intelligent driving systems," *Mathematical Problems in Engineering*, vol. 2019, Article ID 3737486, 10 pages, 2019.